
FREQUENT SUBGRAPH-BASED PERSISTENT HOMOLOGY FOR GRAPH CLASSIFICATION

A PREPRINT

Xinyang Chen

Harbin Institute of Technology, Shenzhen
 Université de Lille, Laboratoire Painlevé (CNRS UMR 8524)
 xinyang.chen.etu@univ-lille.fr

Amaël Broustet

Université de Lille, Laboratoire Painlevé (CNRS UMR 8524)
 amael.broustet@univ-lille.fr

Guoting Chen

Great Bay University, Dongguan, Guangdong, China
 guoting.chen@univ-lille.fr

ABSTRACT

Persistent homology (PH) has recently emerged as a powerful tool for extracting topological features. Integrating PH into both machine learning and deep learning models enhances their topology-awareness and interpretability. However, most PH methods on graphs rely on a limited set of filtrations (e.g., degree- or weight-based), which overlook richer features such as recurring information across the dataset, thereby restricting their expressive power. In this work, we propose a novel filtration on graphs, called *Frequent Subgraph Filtration* (FSF), which is derived from frequent subgraphs and produces stable and information-rich *Frequency-based Persistent Homology* (FPH) features. We explore the theoretical properties of FSF and provide proofs and experimental validation of them. Beyond persistent homology itself, we further introduce two approaches for graph classification: (i) an FPH-based machine learning model (FPH-ML), and (ii) a hybrid framework integrating FPH with graph neural networks (FPH-GNNs) to enhance topology-aware graph representation learning. Our proposed frameworks demonstrate the potential for bridging frequent subgraph mining and topological data analysis, providing a new perspective on topology-aware feature extraction and graph representation learning. Experimental results show that FPH-ML achieves competitive or superior accuracy compared to kernel-based and degree-based filtration methods. When injected into GNNs, FPH delivers relative gains of 0.4–21% (up to +8.2 pts) over their GCN/GIN backbones across benchmarks.

Keywords Frequent subgraph mining · Persistent homology · Filtration · Graph classification

1 Introduction

Graph classification is fundamental to graph learning, with applications in social networks, cheminformatics, and bioinformatics [26]. Existing approaches can be categorized into two main categories: kernel-based and graph neural network (GNN)-based methods [2]. Kernel methods, including random walk [22], graphlet [37], and Weisfeiler–Lehman (WL) kernels [36], offer strong theoretical foundations but scale poorly to large datasets. In contrast, GNNs have emerged as the dominant paradigm, learning graph representations end-to-end and achieving state-of-the-art performance on diverse benchmarks [21, 38]. These models primarily focus on local neighborhood aggregation, effectively capturing local structural information. However, despite these advances, GNNs often struggle to capture global, high-order topological features, which are crucial for distinguishing graphs, especially in domains where topological structure plays a central role.

To overcome these limitations, there has been growing interest in integrating topological data analysis (TDA) with machine learning and GNNs, as graphs are inherently topological structures [19, 32]. Among TDA techniques, Persistent Homology (PH) is a powerful method for extracting multi-dimensional topological features, such as connected components, cycles, and voids. PH tracks the birth and death of these features across a filtration sequence, resulting in persistence diagrams that provide a compact and informative summary of the graph’s topological structure. Unlike GNNs, which primarily focus on local neighbourhood information, PH is capable of capturing global, high-dimensional topological information, offering complementary insights for graph representation and enhancing the interpretability of models.

A key component of PH is the filtration function, which defines the order in which graph elements (nodes or edges) are added to construct a sequence of nested simplicial complexes. Most existing graph filtrations are primarily based on edge weights (e.g., Vietoris-Rips [29], Dowker sink and source filtrations [6]), which limits their applicability to weighted graphs. Other approaches, such as degree-based filtrations, rely on simple local properties of vertices and often fail to capture meaningful global topological structures [2]. However, most existing PH-enhanced GNN methods primarily adopt existing filtrations or learn task-driven filtrations, while neglecting the optimization of PH-internal representations themselves [17, 43]. As a result, the expressive potential of PH is not fully exploited. Therefore, designing more expressive and diverse filtration strategies is essential for enhancing the representational capacity of PH in graph learning tasks.

To address these limitations, we propose a novel graph filtration based on frequent subgraph patterns. Our method mines limited-size frequent patterns across the dataset and constructs a filtration for each graph via isomorphic mapping. This design incorporates recurring structural information and captures global dataset-level topology. We integrate the filtration into both traditional machine learning and GNN pipelines for graph classification. Our main contributions are:

- (i) We propose *Frequent Subgraph Filtration* (FSF), the first frequency-driven filtration for graphs, which integrates frequent subgraph patterns information into persistent homology (PH) to capture recurring, stable, and dataset-level topological information.
- (ii) We explore and prove the theoretical properties of FSF, including the PH dimension (bounded by pattern size), monotonicity, and isomorphism invariance.
- (iii) We introduce two graph classification approaches: (a) a *Frequency-based Persistent Homology* (FPH) machine learning model (FPH-ML), and (b) a hybrid framework integrating FPH with graph neural networks (FPH-GNN) to enhance topology-aware graph representation learning.
- (iv) Extensive experiments on graph classification benchmarks demonstrate that our methods consistently outperform kernel-based baselines, existing PH-based models, and GNNs on most datasets.

The rest of the paper is organized as follows. In section 2, we present work related to this study. Section 3 is devoted to basic definitions. In Section 4, we present a new framework for frequent subgraph filtration. In Section 5, we propose the frequency persistent homology for graph classification. Experimental results are shown in Section 6. Analysis on the limitations and future work is given in Section 7. Finally, Section 8 provides the conclusions

2 Related work

Frequent subgraph mining. Frequent subgraph mining (FSM) is a fundamental graph mining task that discovers recurring substructures in datasets [34]. Early methods, such as AGM [20], follow an Apriori-style candidate generation, but suffer from high costs of repeated subgraph isomorphism tests. To overcome this, gSpan [42] adopts DFS codes with a depth-first extension strategy, while Grami [10] encodes subgraph isomorphism as a constraint satisfaction problem for efficient growth and pruning.

Since not all frequent subgraphs are meaningful, methods like cgSpan [35] and FCSG [4] focus on concise representations. For dynamic graphs, DyFSM [5] uses a fringe set to incrementally update frequent subgraphs as databases evolve, while He et al. [15, 16] propose frameworks for mining sequences in dynamic attributed graphs and extracting credible attribute rules. FSM has also been extended beyond simple graphs. For example, Aslay et al. [3] study hypergraphs, and FreSCo [31] generalizes FSM to simplicial complexes. More recently, learning-based FSM has attracted increasing attention. SPMiner [44] is the first approach to represent subgraphs in a learned embedding space, leveraging order embeddings to preserve the hierarchical relation between subgraphs and their supergraphs. Multi-SPMiner [45] extends this framework to multi-graph settings.

Persistent homology and its application. Topological data analysis (TDA) has gained increasing attention, with persistent homology (PH) as its most widely used tool for tracking topological features across scales [12]. PH quantifies

structures such as connected components, loops, and voids [9], typically summarized in persistence diagrams that record feature birth and death times. To facilitate interpretation, other representations have been developed, including barcodes [40], persistence landscapes [11], and persistence images [1].

PH has been applied in diverse domains, including neuroscience [25], GIScience [7], and time-series analysis [33]. For example, Corcoran and Jones [8] apply PH to GIScience, demonstrating robustness, void detection, and downstream analysis through PH-based signatures. Beyond direct applications, PH has been integrated into machine learning [32] and increasingly combined with deep learning [30]. Persistent homology can enhance neural networks by providing higher-order structural information. For example, Zhao et al. [46] proposed a novel network architecture where PH guides graph neural networks (GNNs) by reweighting message passing between graph nodes. TOGL [17] introduced a topological graph layer based on persistent homology and demonstrated that topological features can improve the expressive power of GNNs. Similarly, Rephine [19] is a framework that extends PH by designing a new refined filtration, enabling richer topological features to be incorporated into graph representation.

Graph classification. Graph classification aims to assign labels to entire graphs. Research has evolved from kernel-based similarity measures to embedding methods and, more recently, expressive and scalable GNNs. Early work focused on graph kernels combined with classifiers such as SVMs [24]. Representative examples include Random Walk Kernels [22], which count matching random walks; Graphlet Kernels [37], which compare distributions of small induced subgraphs; and Weisfeiler–Lehman (WL) Kernels [36], which iteratively relabel neighborhoods to capture richer structures. These methods perform well on small and medium datasets but suffer from high computational cost and poor scalability. To overcome these issues, graph embedding methods learn low-dimensional vector representations without explicit pairwise kernel computation, e.g., Graph2Vec [28] provides fixed-size embeddings for entire graphs.

Graph Neural Networks (GNNs) have recently become the dominant approach for graph classification. They follow the message-passing paradigm, where nodes aggregate information from neighbors and a readout operation produces graph-level embeddings [13]. Representative models include GCNs [23], which apply spectral filtering; GraphSAGE [14], which uses neighborhood sampling for inductive learning; GATs [39], which incorporate self-attention; and GINs [41], which achieve Weisfeiler–Lehman-level discriminative power through expressive aggregation.

Based on the aforementioned literature review, we note that although significant progress has been made in frequent subgraph mining, persistent homology, and graph classification, their integration remains limited. Motivated by these, we integrate FSM and PH to capture globally recurring and higher-order topological information, thereby enabling a more informative representation for graph classification.

3 Preliminaries

A vertex-labeled undirected graph is a tuple $G = (V, E, \ell)$, where V is a finite set of vertices, $E \subseteq \{\{u, v\} \mid u, v \in V, u \neq v\}$ is a set of undirected edges, and $\ell : V \rightarrow L$ is a label function mapping each vertex to a label from a finite label set L . Given two vertex-labeled undirected graphs $G = (V, E, \ell)$ and $G' = (V', E', \ell')$. If there exists a bijection $\phi : V \rightarrow V'$ such that: $(u, v) \in E \Leftrightarrow (\phi(u), \phi(v)) \in E'$, $\ell(u) = \ell'(\phi(u))$ for all $u \in V$, then G and G' are isomorphic, denoted as $G \cong G'$.

We now define MNI-frequent subgraph.

Definition 3.1 (MNI-Frequent Subgraph). Let $\mathcal{D} = (V, E, \ell)$ be a single vertex-labeled undirected graph, and let $g = (V_g, E_g, \ell_g)$ be a vertex-labeled subgraph. An embedding of g in \mathcal{D} is an injective mapping $\phi : V_g \rightarrow V$ that preserves adjacency and vertex labels. We denote by $\text{Emb}(g, \mathcal{D})$ the set of all such embeddings. For each vertex $u \in V_g$, define the distinct node-image set $\text{Img}(u) := \{\phi(u) \mid \phi \in \text{Emb}(g, \mathcal{D})\}$. The Minimum Node Image (MNI) support of g in \mathcal{D} is

$$\text{MNI}(g, \mathcal{D}) = \min_{u \in V_g} |\text{Img}(u)|.$$

Then, g is called *MNI-frequent* if $\text{MNI}(g, \mathcal{D}) \geq \sigma$, where $\sigma \in \mathbb{N}$ is a user-defined minimum support threshold.

Definition 3.2 (Simplicial complex). Let $V = \{v_0, v_1, \dots, v_k\}$ be a set of $k + 1$ affinely independent points. Then, their convex hull is called a k -simplex, where k is the dimension of the simplex:

$$[v_0, v_1, \dots, v_k] = \{x \in \mathbb{R}^n \mid x = \sum_{i=0}^k \lambda_i v_i, \lambda_i \geq 0, \sum_{i=0}^k \lambda_i = 1\}.$$

Let \mathcal{K} be the collection of simplices. If \mathcal{K} satisfies the following two conditions, it is called a simplicial complex:

i) Closure Condition: if $\sigma \in \mathcal{K}$ and τ is any face of σ , then $\tau \in \mathcal{K}$.

ii) Intersection Condition: for all $\sigma, \sigma' \in \mathcal{K}, \sigma \cap \sigma' = \emptyset$ or $\sigma \cap \sigma' \in \mathcal{K}$.

Definition 3.3 (*k*-Chain Group). Given a simplicial complex \mathcal{K} , let \mathcal{K}_k denote the set of all *k*-simplices in \mathcal{K} . The *k*-chain group is defined as:

$$C_k(\mathcal{K}) = \left\{ \sum_i a_i \sigma_i \mid a_i \in \mathbb{Z}, \sigma_i \in \mathcal{K}_k \right\},$$

which forms a free Abelian group generated by the *k*-dimensional simplices.

Definition 3.4 (Boundary Operator). The boundary operator $\partial_p : C_p \rightarrow C_{p-1}$ is defined as:

$$\partial_k(\sigma) = \sum_{i=0}^k (-1)^i [v_0, \dots, \hat{v}_i, \dots, v_k],$$

where $[v_0, \dots, \hat{v}_i, \dots, v_k]$ represents the $(k-1)$ -simplex obtained by removing the *i*-th vertex. An important property of this operator is: $\partial_k \circ \partial_{k+1} = 0, \forall k$. That is, boundaries have no boundary, meaning that each $(k+1)$ -dimensional boundary forms a *k*-dimensional closed chain.

Definition 3.5 (Chain Complex). The boundary operator connects chain groups C_k into a chain complex, given by:

$$\dots \xrightarrow{\partial_{k+2}} C_{k+1} \xrightarrow{\partial_{k+1}} C_k \xrightarrow{\partial_k} C_{k-1} \xrightarrow{\partial_{k-1}} \dots \xrightarrow{\partial_1} C_0 \xrightarrow{\partial_0} 0.$$

Definition 3.6 (*k*-Boundary Group). Given a simplicial complex \mathcal{K} , the *k*-boundary group is defined as:

$$B_k(\mathcal{K}) = \text{Im}(\partial_{k+1}) = \{\partial_{k+1}(\sigma) \mid \sigma \in C_{k+1}\}.$$

Definition 3.7 (*k*-Cycle Group). Given a simplicial complex \mathcal{K} , the *k*-cycle group is defined as:

$$Z_k(\mathcal{K}) = \ker(\partial_k) = \{c \in C_k \mid \partial_k(c) = 0\}.$$

Since $B_k \subset Z_k$ and $Z_k \subset C_k$, this implies that Z_k consists of *k*-cycles (i.e., *k*-closed chains), while B_k consists of *k*-boundaries (i.e., *k*-closed chains that are also boundaries). The goal of homology is to distinguish nontrivial cycles from boundaries, leading to the definition of the homology group:

Definition 3.8 (Homology Group). The *k*-th homology group of a simplicial complex is defined as:

$$H_k(\mathcal{K}) = Z_k(\mathcal{K})/B_k(\mathcal{K}).$$

Its rank is called the Betti number, denoted as β_k , which represents the number of *k*-dimensional nontrivial topological features: $\beta_k = \dim H_k(\mathcal{K})$.

Definition 3.9 (Filtration Sequence). Given a simplicial complex \mathcal{K} , a filtration sequence is a nested sequence of sub-simplicial complexes:

$$\emptyset = \mathcal{K}_{\epsilon_0} \subseteq \mathcal{K}_{\epsilon_1} \subseteq \mathcal{K}_{\epsilon_2} \subseteq \dots \subseteq \mathcal{K}_{\epsilon_n} = \mathcal{K}.$$

Each \mathcal{K}_{ϵ_i} is a subcomplex of \mathcal{K} , and as the scale parameter ϵ increases, the simplicial complex grows. That is,

$$\epsilon_0 \leq \epsilon_1 \leq \dots \leq \epsilon_{n-1} \leq \epsilon_n.$$

Thus, we can introduce the definition of persistent homology:

Definition 3.10 (Persistent Homology). Let \mathcal{K} be a simplicial complex with a filtration sequence $[\mathcal{K}_{\epsilon_0} \subseteq \mathcal{K}_{\epsilon_1} \subseteq \mathcal{K}_{\epsilon_2} \subseteq \dots \subseteq \mathcal{K}_{\epsilon_n}]$. For each $\mathcal{K}_{\epsilon_i} \in \mathcal{K}$, the corresponding *k*-th homology group is $H_k(\mathcal{K}_{\epsilon_i})$. The birth of a topological feature α is defined as its first appearance in \mathcal{K}_{ϵ_b} , and its death is when it disappears in \mathcal{K}_{ϵ_d} . The persistent homology group is then defined as:

$$H_k^{b,d} = \text{Im}(H_k(\mathcal{K}_{\epsilon_b}) \rightarrow H_k(\mathcal{K}_{\epsilon_d})).$$

Definition 3.11 (Persistence Diagram). Given a filtered simplicial complex $\{K_t\}_{t \in \mathbb{R}}$, the *p*-dimensional persistent homology captures the birth and death times of *p*-dimensional topological features as the filtration parameter *t* increases. The persistence diagram PD_p is a multiset of points in \mathbb{R}^2 of the form (b, d) , where *b* and *d* denote the birth time and death time, respectively, of a *p*-dimensional feature, with $b < d \leq \infty$. Features with infinite death time are often treated as points at infinity or capped at a fixed value for computational purposes.

For example, Figure 1 illustrates an example of a filtration sequence, and Figure 2 shows the persistent diagram. For H_0 (red points in the persistent diagram), there are four components at filtration 0, but three of them die at filtration 1. For H_1 (blue points in the persistent diagram), a cycle is born at filtration 2, and it dies at filtration 3 because two 2-simplices are added to kill it.

Definition 3.12 (Bottleneck Distance). Let D_1 and D_2 be two persistence diagrams. The bottleneck distance between D_1 and D_2 is defined as

$$d_B(D_1, D_2) = \inf_{\gamma} \sup_{x \in D_1} \|x - \gamma(x)\|_{\infty},$$

where γ ranges over all bijections between D_1 and D_2 , and $\|\cdot\|_{\infty}$ denotes the ℓ_{∞} norm. Intuitively, the bottleneck distance measures the largest shift needed to match the points of one diagram to the other.

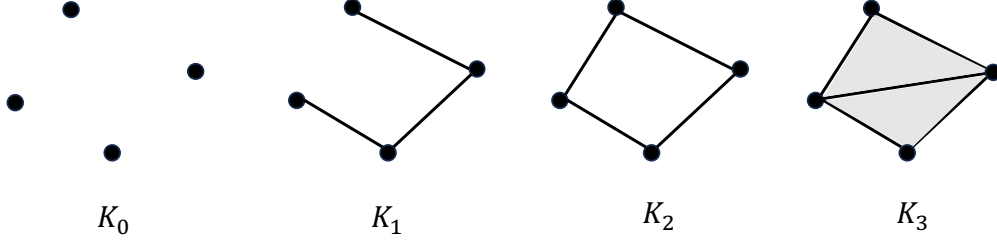


Figure 1: Example of filtration.

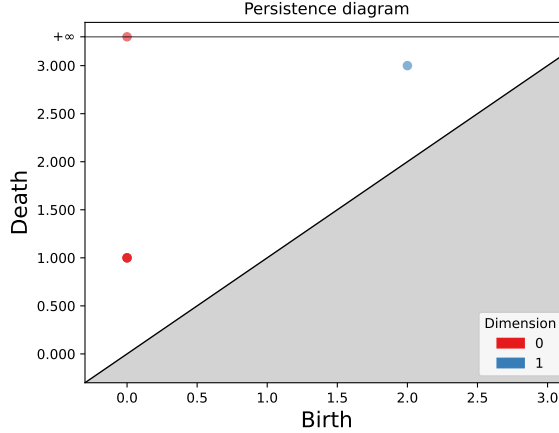


Figure 2: Example of persistence diagram.

4 Frequent subgraph-based filtration

We now propose a novel filtration method constructed from frequent subgraph patterns. The framework for filtration construction is shown in Figure 3. Given a vertex-labeled graph transaction dataset $\mathcal{D} = \{G_0, G_1, \dots, G_n\}$, we consider the union of all graphs as a large graph \mathcal{G} , which serves as the input for FSM. We now formalize the k -size Frequent Subgraph Mining (k-FSM) problem.

Figure 3 illustrates the overall process of the filtration construction.

Problem (k-size Frequent Subgraph Mining (k-FSM))

Given a user-defined minimum support threshold $\sigma \in \mathbb{N}$ and a maximum subgraph size k (where size refers to the number of vertices in the subgraph), the goal of k-FSM is to discover all subgraphs of size at most k that are MNI frequent subgraph (Definition 3.1) in \mathcal{G} . Formally, a subgraph g is considered k-size frequent if:

$$\mathcal{F}_k(\mathcal{G}, \sigma) = \{g \in \mathcal{G}_k \mid \text{MNI}(g, \mathcal{G}) \geq \sigma, |V_g| \leq k\}.$$

We perform k-FSM on \mathcal{G} to obtain a collection of frequent subgraph patterns, denoted as P_{ij} , where i indexes the subgraph pattern and j corresponds to the frequency threshold level. Subsequently, for each graph G_i , we extract the set of vertices that participate in the isomorphisms of frequent subgraph patterns. These vertex sets are then treated as simplices to construct a simplicial complex for G_i . This complex encodes high-order topological relationships among frequently co-occurring vertex groups, thus capturing richer structural information. Finally, we define a filtration by progressively adding simplices to the complex based on the decreasing order of their corresponding subgraph frequency. This process results in a k-FSF sequence for each graph G_i .

Definition 4.1 (k-size Frequent Subgraph-Based Filtration (k-FSF)). Let \mathcal{D} be a graph transaction dataset and let $G \in \mathcal{D}$ be a graph. Let P_t denote the set of frequent subgraph patterns whose dataset-level frequency satisfies $\text{MNI}(p, \mathcal{D}) \geq \frac{1}{t}$ and $|V_p| \leq k$.

For a filtration value $t \in \mathbb{R}_+$, we define the simplicial complex \mathcal{K}_t on G as

$$\mathcal{K}_t = \left\{ \Delta(\varphi(V_p)) \mid p \in P_t, \varphi \in \text{Emb}(p, G) \right\},$$

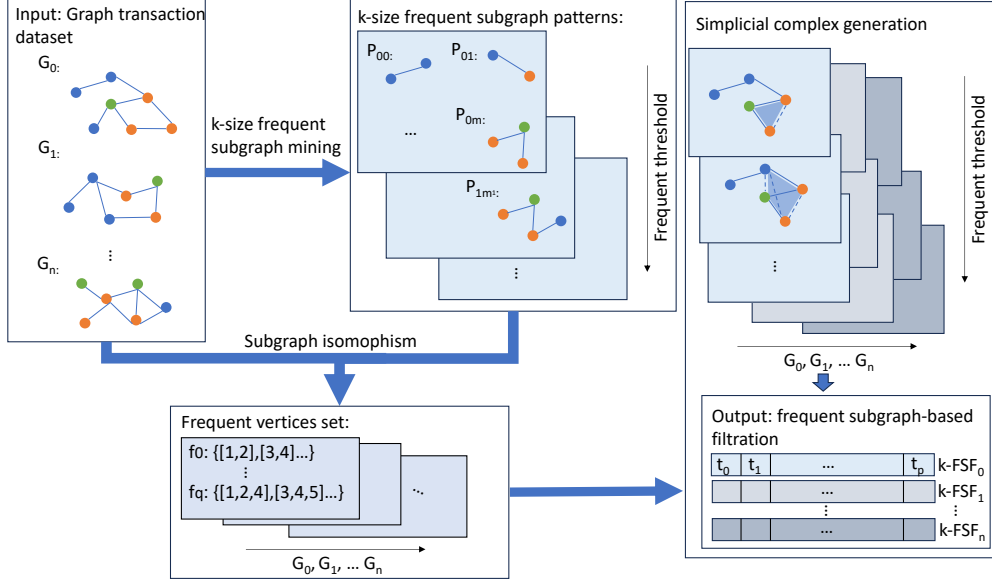


Figure 3: k-FSF construction.

where $\Delta(S)$ denotes the simplex spanned by the vertex set S , $\text{Emb}(p, G)$ denotes the set of all vertex-label-preserving subgraph isomorphisms (embeddings) of pattern p into G , and $\varphi(V_p) \subseteq V(G)$ is the vertex image set induced by an embedding φ .

The k-FSF filtration is then defined as the nested family $\{\mathcal{K}_t\}_{t \in \mathbb{R}_+}$. As t increases (equivalently, as the threshold $1/t$ decreases), more simplices are progressively added to the complex, thereby enlarging the topological structure.

Figure 4 illustrates an example of k -FSF $\{\mathcal{K}_t\}_{t_0 < t_1 < t_2}$. Figures 4(a)-4(c) show the simplicial complexes at times t_0 , t_1 , and t_2 , respectively. As t increases, additional simplices are incorporated, enriching the topology. For example, the isolated component $[730, 731]$ at t_0 becomes connected to the main complex at t_1 through 1-simplices $[713, 730]$, $[714, 730]$, and $[713, 731]$, as well as a 2-simplex $[713, 714, 716]$. At t_2 , further 2-simplices, such as $[713, 730, 716]$, are added, increasing topological complexity.

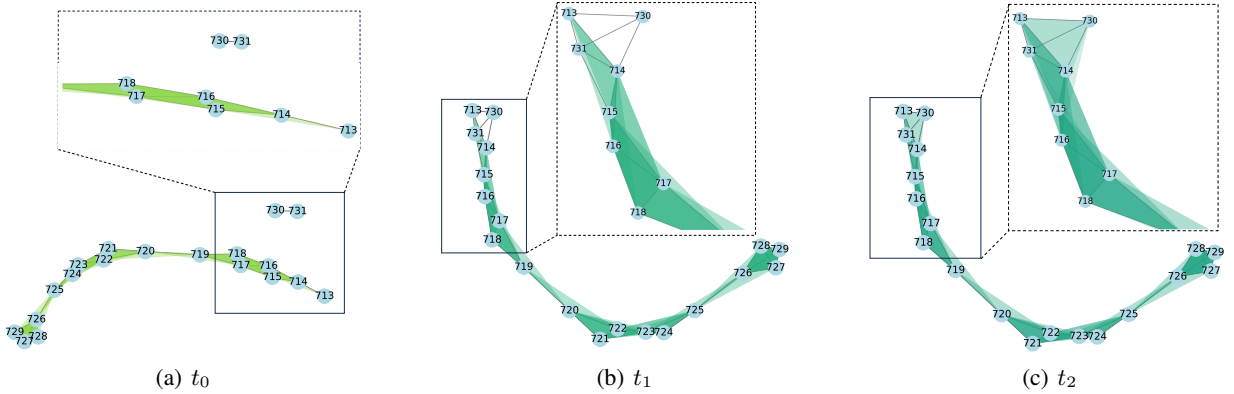


Figure 4: Example of k-FSF.

Here, we give three propositions on FSF, and the formal proofs are provided.

Proposition 4.2 (Homology Dimension of k-FSF). *Let $\{\mathcal{K}_t\}_{t \in \mathbb{R}_+}$ be a k-FSF on a graph G . Then the maximum dimension $\max D$ in which persistent homology can be nontrivial is bounded by:*

$$\max D = \max\{p \in \mathbb{N} \mid H_p(\mathcal{K}_t) \neq 0\} \leq k - 1.$$

Moreover, for $t_1 \leq t_2$, the persistent map $H_{k-1}(\mathcal{K}_{t_1}) \rightarrow H_{k-1}(\mathcal{K}_{t_2})$ is injective.

Proof. For every frequent subgraph pattern p , if it is isomorphic with a subgraph of G , it contributes to vertex sets $T \subset I(V_p)$ of size at most k , which induces simplexes $\Delta(T)$ of dimension at most $k - 1$. Thus, for every simplex $\sigma \in \mathcal{K}_t$, the dimension $\dim(\sigma) \leq k - 1$. Let $C_p(\mathcal{K}_t)$ be the p -chain group. Then, we have $C_p(\mathcal{K}_t) = 0$ for all $p \geq k$. By the definition of p -th homology group, $H_p(\mathcal{K}_t) = \ker(\partial_p) / \text{Im}(\partial_{p+1})$, where $\partial_p : C_p \rightarrow C_{p-1}$ is the boundary operator. We have $H_p(\mathcal{K}_t) = 0$ for all $p \geq k$. Therefore, the maximum dimension for nontrivial persistent homology is $k - 1$.

Furthermore, for $p = k - 1$, the image of the boundary operator ∂_k is 0 (as $C_k = 0$). Hence, $\text{Im}(\partial_k) = 0$. Then we have $H_{k-1} = \ker(\partial_{k-1})$. This implies that any $(k - 1)$ -hole, once formed, cannot be filled by higher-dimensional simplices. Therefore, such classes persist indefinitely in the filtration. \square

Note that even for homology groups other than H_{k-1} , the groups $H_i(\mathcal{K}_t)$ need not vanish for $t \gg 1$. This contrasts with what happens in filtrations such as Vietoris-Rips.

Example of non-vanishing. As shown in Figure 5, we subdivide the edges $\{a, b\}, \{a, c\}, \{b, c\}$ by introducing the vertices d, e, f , respectively. If the pattern size is equal to 3, $\forall t \gg 1$, the complex \mathcal{K}_t contains the following 2-simplices as well as their subsimplices: $\triangle abd, \triangle ace, \triangle ade, \triangle bcf, \triangle bdf$, and $\triangle cef$.

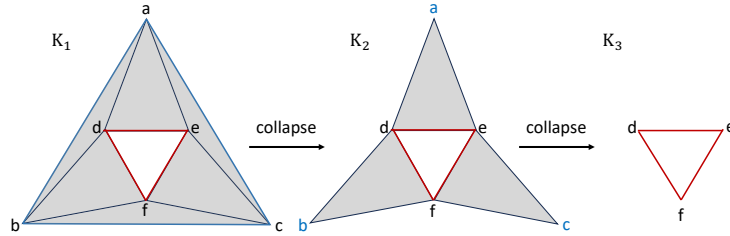


Figure 5: Example of non-vanishing.

Considering H_1 , in the complex \mathcal{K}_1 the 1-simplex $\{a, b\}$ is only contained in the 2-simplex $\triangle abc$, hence it is a free face; the same holds for $\{a, c\}$ and $\{b, c\}$. By performing elementary collapses on these free faces, we obtain the reduced complex \mathcal{K}_2 .

In \mathcal{K}_2 , the vertices a, b, c become free faces contained uniquely in $\triangle ade, \triangle dbf$, and $\triangle efc$, respectively. Collapsing them gives the final reduced complex \mathcal{K}_3 .

Therefore, we conclude that

$$H_1(\mathcal{K}_1) \cong H_1(\mathcal{K}_3) \neq 0.$$

This shows that persistence obtained from FSF is not only a consequence of the frequency of patterns but also of the topology of the graph.

Proposition 4.3 (Monotonicity of FSF). *Let $\{\mathcal{K}_t\}_{t \in \mathbb{R}_+}$ be k -FSF constructed on a graph G . Then the filtration is monotonic with respect to t , i.e.,*

$$\mathcal{K}_{t_1} \subseteq \mathcal{K}_{t_2} \subseteq \dots \subseteq \mathcal{K}_{t_n} = \mathcal{K} \quad \text{for } t_1 < t_2 < \dots < t_n.$$

Proof. As t increases, the frequency threshold $\theta = \frac{1}{t}$ decreases, allowing more subgraph patterns to be considered frequent:

$$t_1 < t_2 \quad \Rightarrow \quad \frac{1}{t_1} > \frac{1}{t_2} \quad \Rightarrow \quad P_{t_1} \subseteq P_{t_2},$$

where P_t denotes the set of subgraph patterns frequent at threshold $1/t$.

For each frequent subgraph pattern $p \in P_t$, let $\text{Emb}(p, G)$ denote the set of all isomorphic embeddings of p into G . Each such embedding induces a vertex set $T \subseteq V(G)$, which defines a simplex $\Delta(T)$ in the simplicial complex. Thus, as t increases, more subgraph patterns and their embeddings are included, contributing additional simplices to the complex:

$$\mathcal{K}_{t_1} \subseteq \mathcal{K}_{t_2}, \quad \text{for all } t_1 < t_2.$$

Hence, the filtration is monotonic in t . \square

Proposition 4.4 (FSF is Isomorphism Invariant). *Let G and G' be two isomorphic vertex-labeled graphs, written $G \cong G'$. Then the FSFs constructed from G and G' are isomorphic; that is, for each filtration step i ,*

$$\mathcal{K}_i \cong \mathcal{K}'_i,$$

where \mathcal{K}_i denotes the simplicial complex at filtration value i . Consequently, the persistence diagrams of G and G' are equal:

$$D_G = D_{G'}.$$

Proof. Let G and G' be two graphs such that $G \cong G'$. Let $\phi : V(G) \rightarrow V(G')$ be a vertex-label-preserving graph isomorphism. For any subgraph $S \subseteq G$, there exists an isomorphic subgraph $\phi(S) \subseteq G'$. This subgraph $\phi(S)$ induces the corresponding vertex set $V_{\phi(S)}$. Hence, under the same frequent subgraph threshold, the sets of frequent subgraph vertices coincide, i.e., $V_{S \subseteq G} = V_{\phi(S) \subseteq G'}$. Therefore, at each step of the filtration, an isomorphic simplicial complex is obtained. In particular, the filtration $\{\mathcal{K}'_t\}_{t \in \mathbb{R}_+}$ on G' satisfies $\mathcal{K}_t \cong \mathcal{K}'_t$ for all t . Thus, the persistence diagrams are identical: $D_G = D_{G'}$. \square

5 Frequency persistent homology for graph classification

In this section, we show how FPH features enhance graph classification through two approaches: (i) an FPH-based machine learning model, and (ii) integrating FPH with GNNs for enhancing topology-aware representation learning.

5.1 FPH-based machine learning

Figure 6 illustrates the FPH-based machine learning (FPH-ML) pipeline. FPH features are extracted via the proposed k -FSF, vectorized into PH statistical features, and used as classifier inputs. Unlike graph kernels or GNNs, this approach relies solely on topological statistics from persistent homology, without kernels or message passing.

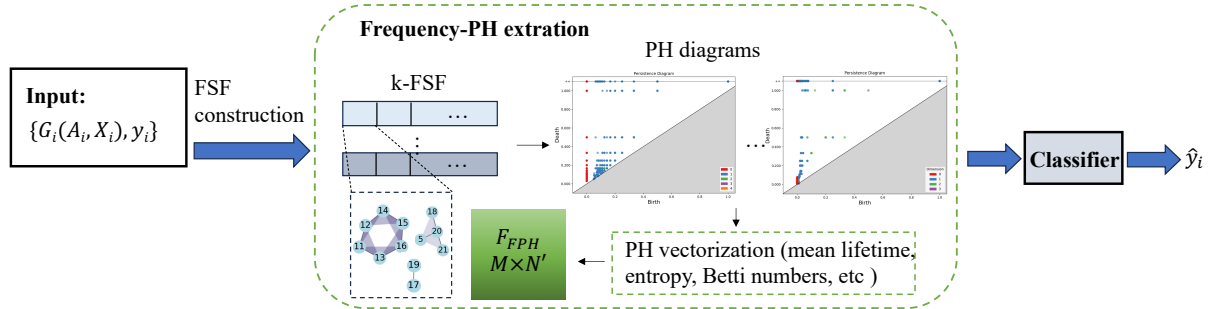


Figure 6: FPH-ML pipeline.

For each homology dimension $k \in \{0, \dots, d\}$ of graph G_i , let $\text{PD}_i^k = \{(b_j^k, d_j^k)\}_{j=1}^{n_k}$ denote the persistence pairs, where infinite values are set to 1. The lifetime of each pair is $\ell_j^k = d_j^k - b_j^k$, and if $n_k = 0$, the features are zero-padded. From the lifetimes, we compute seven statistics: mean (μ), maximum (L_{\max}), minimum (L_{\min}), median (\tilde{L}), standard deviation (σ), Betti number (β), and entropy (E). The total persistence across all finite pairs is $P_{\text{tot},i} = \sum_{(b,d): d < \infty} (d - b)$. Concatenating features across all dimensions yields the PH vector

$$\mathbf{f}_i = [\mu_i^0, L_{\max,i}^0, L_{\min,i}^0, \tilde{L}_i^0, \sigma_i^0, \beta_i^0, E_i^0, \dots, \mu_i^d, L_{\max,i}^d, L_{\min,i}^d, \tilde{L}_i^d, \sigma_i^d, \beta_i^d, E_i^d, P_{\text{tot},i}].$$

We have $\mathbf{f}_i \in \mathbb{R}^{7(d+1)+1}$. Then, all the \mathbf{f}_i are stacked as the graph embedding with dimension $M \times N'$:

$$F_{\text{FPH}} = [f_1; f_2; \dots; f_M] \in \mathbb{R}^{M \times N'}.$$

We then train a classifier $h : \mathbb{R}^{N'} \rightarrow \mathcal{Y}$ such that $\hat{y}_i = h(f_i)$.

5.2 Combining FPH with GNNs

We develop FPH-GNN to enhance the expressiveness of GNN-based graph embeddings by integrating global, stable, and high-order topological information. Figure 7 illustrates the overall framework. Specifically, the FPH features are

incorporated into the original graph input as a global PH token, guiding the GNN to be aware of global topological structure beyond local message passing. The input consists of a set of graphs $\{G_i(A_i, X_i, Y_i)\}_{i=1}^M$, where A_i denotes the adjacency matrix, X_i the node feature matrix, and y_i the corresponding graph label. The key components of the framework are detailed below.

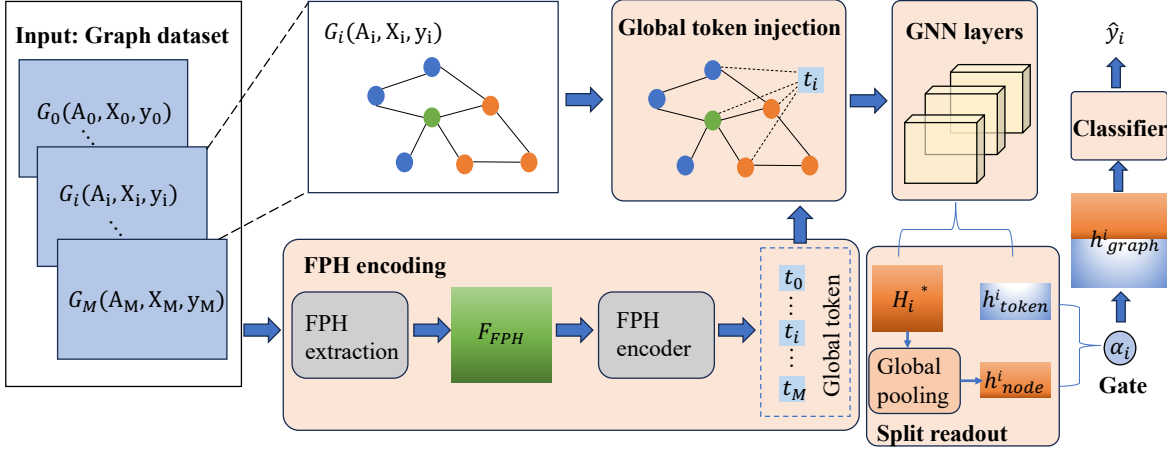


Figure 7: Overview of the proposed FPH-GNN framework.

FPH encoding. For each graph G_i , we precompute its topological feature $F_{\text{FPH}}^i \in \mathbb{R}^{d_{\text{ph}}}$. To align these topological features with the latent representation space of node embeddings, we employ a multi-layer perceptron (MLP) as an encoder. Then the FPH embedding is obtained:

$$e_{\text{fph}}^i = \text{MLP}(F_{\text{FPH}}^i) \in \mathbb{R}^H,$$

where H denotes the hidden dimension.

Global token injection. The encoded FPH embedding e_{fph}^i is injected into G_i as a virtual global token node t_i to serve as a global representative of topological knowledge. To maximize its influence, t_i is connected to the top- K highest-degree nodes in G_i , forming edges (t_i, v) where $v \in \text{TopKDeg}(G_i)$. Consequently, $H_i^{(0)} \in \mathbb{R}^{n_i \times d}$ incorporates both node features and the injected FPH token, enabling subsequent GNN layers to jointly propagate global topological context alongside local structural information.

GNN layers: We use L layers of GNN to propagate both structural and topological information:

$$H_i^{(l)} = \text{GNN}^{(l)}(A_i^l, H_i^{(l-1)}) \quad \text{for } l = 1, \dots, L,$$

where A_i^l is the new adjacency including the FPH token, and $H_i^{(l)} \in \mathbb{R}^{n_i \times d}$ denotes the hidden node representations. Finally, to guarantee that the encoded FPH features are not overshadowed or diminished after multiple layers of message passing, we use a residual skip connection mechanism from the initial embedding $H_i^{(0)}$ to the final representation $H_i^{(L)}$:

$$H_i^* = \text{ReLU}(H_i^{(0)} + H_i^{(L)}).$$

Split readout and gated fusion. After L GNN layers, we separately read out the representations of ordinary nodes and the FPH token. Since each graph has only one token node, its representation is $h_{\text{token}}^i = H_{i,t_i}^*$. For the ordinary nodes, we apply a permutation-invariant READOUT function (e.g., global sum pooling):

$$h_{\text{node}}^i = \text{READOUT}(\{H_{i,v}^* : v \in V_i\}).$$

To adaptively fuse structural and topological information, we compute a gate coefficient α_i via an MLP:

$$\alpha_i = \sigma(\text{MLP}_{\text{gate}}(F_{\text{FPH}}^i)), \quad h_{\text{graph}}^i = h_{\text{node}}^i + \alpha_i h_{\text{token}}^i.$$

The fused representation h_{graph}^i is then fed to a classifier over C classes, yielding $\hat{y}_i \in \mathbb{R}^C$.

Overall, FPH-GNN combines local structure captured by the GNN with global topological signals from FPH, enabling topology-aware graph representations.

6 Experiments

We conduct a series of experiments to assess our proposed approach: (1) the robustness of FSF, (2) the performance of FPH-ML, which reveals the discriminative power of FPH features, and (3) the performance of the proposed FPH-GNN framework. Here, we set $k = 4$, which obtains the maximum PH dimension H_3 (Proposition 4.2). We consider that H_3 (once born, never killed) is less informative. Thus, our FPH combines H_0 , H_1 , and H_2 .

The datasets used in our experiments are sourced from the publicly available TUDataset collection [27], available at <https://chrsmrrs.github.io/datasets/> and the Open Graph Benchmark (OGB) [18]. Table 1 shows the statistics of datasets. Here, $|G|$ denotes the number of graphs, $|AN|$ the average number of nodes, $|AE|$ the average number of edges, $|VL|$ is the number of node labels, and *Classes* the number of target classes for each dataset. The implementation is based on PyTorch, and we employ the GUDHI library for persistent homology computations. To explore the frequent subgraph patterns, we use *gSpan*-based method. All experiments are performed on a CPU workstation equipped with an Intel Core i9 processor and 32 GB of RAM.

Table 1: Dataset statistics.

Dataset	$ G $	$ AN $	$ AE $	$ VL $	Classes
AIDS	2000	15.69	16.20	2	2
PROTEINS	1113	39.06	72.82	3	2
NCI1	4110	29.87	32.30	37	2
ENZYMES	600	32.63	62.14	3	6
DD	1178	284.32	715.66	89	2
ogbg-molhiv	41127	25.5	27.4	119	2

6.1 Robustness of FSF

To assess FSF robustness, we perturb graphs by randomly adding or removing edges and measure changes via the bottleneck distance between the original and perturbed persistence diagrams. Experiments consider H_1 and H_2 on PROTEINS, NCI1, and AIDS, with perturbations of edge removal (R) or addition (A) at ratios 0.05 and 0.1 of total edges.

Figure 8 shows the persistent diagram of the original graph and the perturbed graphs across these three datasets, and Table 2 illustrates the bottleneck distance (definition 3.12) results. As shown in table 2, the bottleneck distances for all datasets and perturbation settings remain extremely small, typically on the order of 10^{-4} to 10^{-2} . For example, for PROTEINS, the distances for H_1 remain below 1.1×10^{-3} even with a 0.1 perturbation ratio, and for H_2 they remain under 2×10^{-3} . Across all three datasets, increasing the perturbation ratio from 0.05 to 0.1 leads to only minor increases in bottleneck distance. For instance, in NCI1, H_1 exhibits an increase of only about 2×10^{-3} for edge removal, while the increase for H_2 is about 5×10^{-3} . The performance shows a similar trend for edge addition.

Table 2: Bottleneck distances for H_1 and H_2 .

Dataset	H-dim	R_0.05	R_0.1	A_0.5	A_0.1
PROTEINS	H_1	9.797×10^{-4}	1.029×10^{-3}	9.629×10^{-4}	9.629×10^{-4}
	H_2	1.604×10^{-3}	1.953×10^{-3}	9.573×10^{-4}	1.719×10^{-3}
NCI1	H_1	5.562×10^{-3}	7.221×10^{-3}	1.834×10^{-2}	1.936×10^{-2}
	H_2	4.819×10^{-3}	9.402×10^{-3}	2.230×10^{-2}	2.276×10^{-2}
AIDS	H_1	5.231×10^{-3}	1.907×10^{-2}	1.435×10^{-2}	1.436×10^{-2}
	H_2	1.245×10^{-2}	1.246×10^{-2}	1.351×10^{-2}	1.355×10^{-2}

The results demonstrate that the FSF is highly stable under both edge removal and addition, reflecting its robustness to structural noise. This robustness arises because the filtration is constructed from frequent subgraph patterns mined from the dataset, which capture stable and recurring topological structures.

6.2 Discriminability power of FPH features

FPH-ML performance. We evaluate the performance of FPH-ML to assess the discriminability power of FPH features using a support vector classifier (SVC). We tried both linear and Radial basis function (RBF) kernel and observed

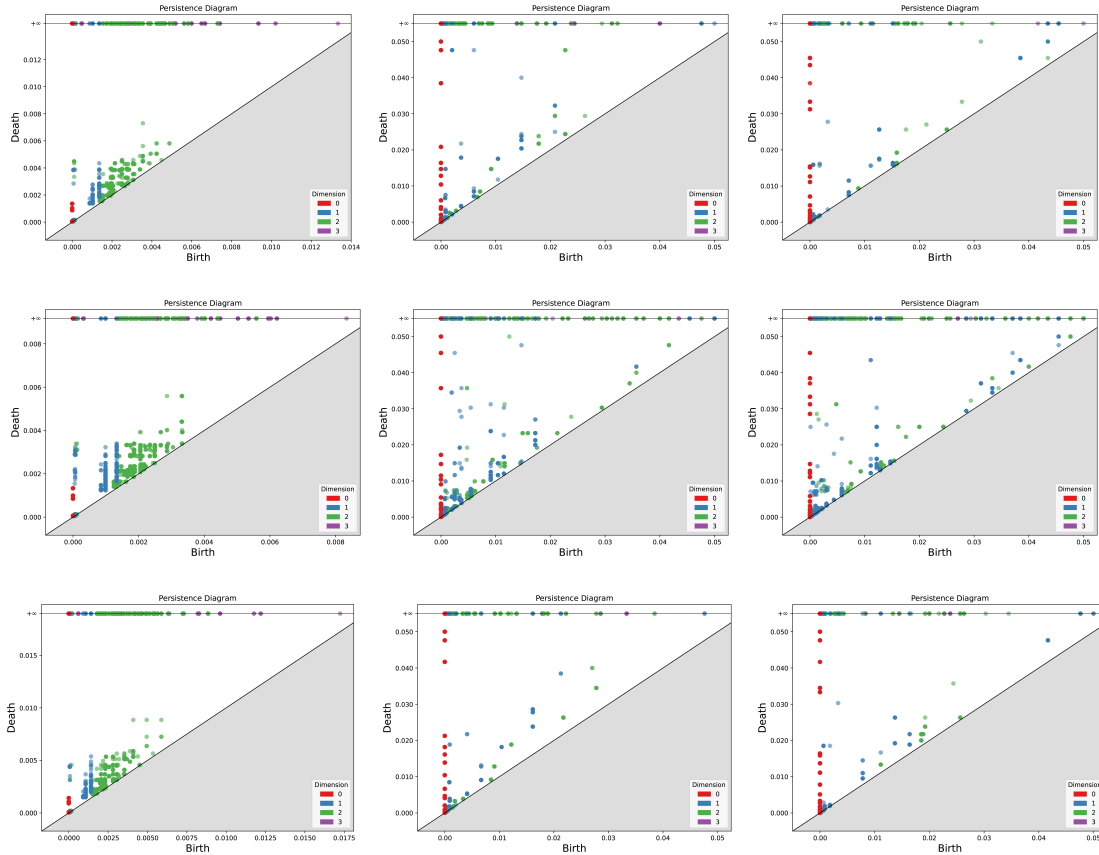


Figure 8: Persistence diagrams for three datasets under different perturbations. Row 1: Original graphs. Row 2: Graphs after adding 10% of edges. Row 3: Graphs after removing 10% of edges. Column 1: PROTEINS. Column 2: AIDS. Column 3: NCI1.

that RBF consistently performed better, thus we use RBF as the kernel. We compare FPH against two baselines: (i) degree-based PH (DPH) and (ii) the Weisfeiler–Lehman (WL) kernel. Additionally, comparing with random-label experiments (FPH-RL and DPH-RL) further confirms that the performance is not due to chance or label distributions.

For each dataset, we use the same 10-fold cross-validation and perform an inner 3-fold cross-validation on the training fold to tune the SVM hyperparameters via GridSearchCV. The best hyperparameters selected on the inner folds are then used to retrain the SVM on the full training fold, and the resulting model is evaluated on the test fold. We report the mean and standard deviation of test accuracy over all 10 folds.

Table 3: Classification accuracy (%) on benchmark datasets using SVC. A **bold** value indicates the best performance for each dataset.

Methods	Datasets				
	PROTEINS	AIDS	NCI1	DD	ENZYMES
FPH	74.31 ± 4.78	99.65 ± 0.59	70.00 ± 1.90	76.65 ± 3.21	36.67 ± 5.37
DPH	69.90 ± 4.89	97.50 ± 1.20	61.71 ± 1.59	74.53 ± 2.84	20.83 ± 5.39
WL	72.04 ± 3.36	98.30 ± 0.75	74.52 ± 2.85	76.12 ± 2.63	51.50 ± 6.34
FPH-RL	50.03 ± 4.54	51.06 ± 5.82	46.01 ± 3.72	43.07 ± 3.93	17.74 ± 3.72
DPH-RL	48.05 ± 3.62	52.01 ± 4.76	48.08 ± 5.83	47.02 ± 3.66	16.03 ± 4.04

Table 3 presents the results. FPH demonstrates superior performance compared to DPH across all datasets, achieving the best accuracy in PROTEINS, AIDS, and DD. For instance, on the PROTEINS dataset, FPH reaches 74.31%, compared to 69.90% with DPH. WL is competitive and achieves the highest performance on NCI1 (74.52%) and ENZYMES (51.50%), surpassing FPH. The random-label baselines yield drastic performance drops for both FPH and DPH, with accuracies around 16% for 6-class classification, while 50% for binary classification, which is close

to random guessing. These results show that the discriminative power of FPH-ML is not due to chance or label distribution, but the inherent strength of FPH features in graph classification tasks.

Contribution of different homology dimensions. To further assess the power of FPH and the contribution of different homology dimensions, we set $k = 5$, which yields H_3 features that can potentially be killed. We evaluate six ablated variants of FPH-ML: (i) combining H_0 – H_2 (H_{0-2}), (ii) combining H_0 – H_3 (H_{0-3}), and (iii) using each of H_0 , H_1 , H_2 , or H_3 individually.

Table 4: Classification accuracy (%) on benchmark datasets using SVC. Gray cells and **bold** values denote the best performance of combined FPH and individual dimensions, respectively.

FPH	Datasets				
	PROTEINS	AIDS	NCII	DD	ENZYMES
H_{0-2}	74.31 ± 4.78	99.65 ± 0.59	70.00 ± 1.90	76.65 ± 3.21	36.67 ± 5.37
H_{0-3}	73.85 ± 3.56	99.60 ± 0.62	69.83 ± 2.17	76.23 ± 2.05	39.50 ± 5.37
H_0	73.05 ± 4.36	99.60 ± 0.70	66.69 ± 1.37	75.04 ± 2.83	27.83 ± 4.60
H_1	73.23 ± 3.57	90.10 ± 1.83	65.84 ± 1.92	76.23 ± 2.17	27.33 ± 6.37
H_2	66.13 ± 4.79	80.00 ± 0.00	60.29 ± 1.81	74.79 ± 2.61	29.93 ± 5.49
H_3	64.96 ± 4.63	80.25 ± 1.33	55.65 ± 1.71	74.02 ± 3.35	32.83 ± 3.80

Results in Table 4 show that H_{0-2} slightly outperforms H_{0-3} on most datasets except ENZYMES, and reveal that different datasets rely on different topological characteristics. For instance, on AIDS and NCII, H_0 dominates, suggesting the importance of connected components, while on PROTEINS and DD, H_1 achieves the best accuracy, highlighting the role of cycle-related features. In contrast, ENZYMES benefits most from H_3 , corresponding to tetrahedral structures.

Discussion. Since ENZYMES benefits most from higher-order homology, we conducted an additional experiment with H_4 and H_{0-4} , achieving 29.33% and **40.83%**, respectively. This reveals that ENZYMES is closely related to higher-order topological structures. However, increasing k will raise the computational cost of both FSM and PH calculation, and H_{0-2} is generally sufficient for most datasets. Therefore, we adopt H_{0-2} as the final FPH configuration. These results provide a clearer understanding of the role of topological features in graph classification, enhancing the interpretability.

Table 5: Classification accuracy (%) on benchmark datasets using GNN-based models. A **bold** value indicates the best performance for each dataset. A gray background indicates better performance between the model and its corresponding baseline.

Methods	Datasets				
	PROTEINS	AIDS	NCII	DD	ENZYMES
FPH-GCN	78.61 ± 3.83	99.65 ± 0.50	78.66 ± 2.36	82.94 ± 3.49	47.00 ± 6.32
DPH-GCN	75.81 ± 4.63	99.25 ± 0.50	75.36 ± 2.96	76.98 ± 4.13	39.81 ± 8.12
GCN	74.48 ± 1.73	99.25 ± 0.63	74.52 ± 1.13	75.66 ± 2.36	38.82 ± 3.31
FPH-GIN	78.80 ± 3.89	99.65 ± 0.63	79.08 ± 2.45	81.92 ± 2.51	44.67 ± 5.57
DPH-GIN	76.35 ± 2.67	99.65 ± 0.56	75.88 ± 4.21	76.52 ± 3.23	42.17 ± 3.29
GIN	76.16 ± 2.76	99.25 ± 0.53	75.52 ± 2.23	76.05 ± 3.60	42.15 ± 3.63
GAT	74.72 ± 4.01	99.00 ± 0.75	74.90 ± 1.83	77.30 ± 3.68	39.83 ± 3.68
GraphSAGE	74.01 ± 4.27	98.20 ± 1.05	74.73 ± 1.63	75.78 ± 3.98	37.93 ± 3.78
Top- k Pool	75.03 ± 1.29	97.25 ± 0.45	78.92 ± 2.14	76.95 ± 2.09	38.35 ± 3.65
RePHINE	72.32 ± 1.89	–	80.92 ± 1.92	–	–

6.3 FPH-GNN performance

In this experiment, we evaluate the performance of the proposed FPH-GNN on five widely used benchmark datasets. The baselines include classical GNN models: GCN, GIN, GraphSAGE, GAT, a pooling-based method Top- k Pool, a persistent homology-based GNN model RePHINE [19] and the degree-based persistent homology model (DPH-GNN). The FPH features are integrated as a plug-in to the GNN models to enhance topology awareness. We perform 10-fold cross-validation, and Table 5 shows the mean classification accuracy with standard deviation.

The experimental results demonstrate that FPH-GNN models consistently outperform their baseline methods across all benchmarks. For example, FPH-GIN achieves the best performance (78.80%) on PROTEINS, compared to 76.16%

for baseline GIN. Furthermore, FPH-GCN attains the best classification accuracy on AIDS (99.65%), DD (82.94%), and ENZYMES (47.00%), surpassing all baselines. On the NCI1 dataset, however, RePHINE slightly outperforms our proposed method. FPH-GCN and FPH-GIN achieve 78.66% and 79.09%, respectively, while RePHINE attains the best performance with 80.92%.

Overall, the experiment results reveal that incorporating FPH features provides complementary global topological information, which can enhance graph-level representation learning, leading to more discriminative performance compared to purely local message-passing approaches.

6.4 Ablation study of FPH-GNN

To assess the contribution of different components in our proposed FPH-GNN models, we conduct comprehensive ablation studies on PROTEINS, AIDS, NCI1, DD, and ENZYMES, considering both FPH-GCN and FPH-GIN models. We evaluate three ablated versions of our model: (i) No Gate (NG): removing the fusion gate α and directly summing node and token representations; (ii) Full Connection (FC): replacing the top- k token injection strategy with full connections from the global topology token to all nodes; (iii) No Residual skip connection (NRsc): eliminating the residual skip connection in the last layer.

Table 6: Ablation study for FPH-GNN.

Methods	Datasets				
	PROTEINS	AIDS	NCI1	DD	ENZYMES
FPH-GCN	78.61 ± 3.83	99.65 ± 0.50	78.66 ± 2.36	82.94 ± 3.49	47.00 ± 6.32
FPH-GCN-NG	78.08 ± 4.65	99.60 ± 0.62	77.92 ± 4.62	81.36 ± 2.42	45.67 ± 5.88
FPH-GCN-FC	78.52 ± 3.95	99.60 ± 0.62	77.79 ± 2.55	81.49 ± 2.99	42.33 ± 5.73
FPH-GCN-NRsc	78.35 ± 3.31	99.60 ± 0.62	78.64 ± 1.70	82.30 ± 3.04	45.17 ± 4.91
GCN	74.48 ± 1.73	99.25 ± 0.63	74.52 ± 1.13	75.66 ± 2.36	38.82 ± 3.31
FPH-GIN	78.80 ± 3.89	99.65 ± 0.63	79.08 ± 2.45	81.92 ± 2.51	44.67 ± 5.57
FPH-GIN-NG	76.98 ± 4.58	99.55 ± 0.60	78.25 ± 2.80	80.90 ± 2.98	43.50 ± 7.32
FPH-GIN-FC	78.38 ± 4.78	99.55 ± 0.61	78.22 ± 1.16	77.93 ± 1.96	40.67 ± 7.23
FPH-GIN-NRsc	77.98 ± 5.35	99.55 ± 0.65	78.35 ± 2.25	79.23 ± 2.98	43.25 ± 5.58
GIN	76.16 ± 2.76	99.25 ± 0.53	75.52 ± 2.23	76.05 ± 3.60	42.15 ± 3.63

As shown in Table 6, removing any of these modules consistently reduces performance compared to the full FPH-GNN. These results highlight the importance of each design choice. For instance, directly summing graph and token embeddings (NG) leads to performance drops, since it removes the adaptive fusion of global and local features. Similarly, fully connecting the global topology token (FC) may introduce noise, thereby reducing the informative role of FPH features. The residual connection (NRsc) also proves essential, as it enhances the influence of FPH features after several GNN layers.

A noteworthy observation is that ablating these modules degrades performance less severely than removing the FPH features themselves, demonstrating that FPH features are the key factor driving the improvement of FPH-GNN over plain GNN baselines.

Frequency features only. To further assess the contribution of PH, we conduct an additional feature-replacement study in which FPH features are replaced by frequency features only. Specifically, we select the top-20 frequent subgraphs identified in the previous FSM step and recompute their MNI frequency in each graph. This results in a 20-dimensional MNI-based feature vector for each graph.

As shown in Table 7, using frequency features of the top-20 frequent subgraphs already yields competitive performance across all three datasets, indicating that frequent subgraph statistics capture meaningful discriminative information. Nevertheless, FPH-GIN consistently outperforms the frequency-only methods. This indicates that FPH offers complementary information beyond frequency counts by encoding richer topological and structural relationships through persistent homology.

Table 7: Replacing FPH with MNI-based frequency features.

Methods	PROTEINS	ENZYMES	NCI1
Top-20 FS-GIN	77.36 \pm 3.84	42.17 \pm 9.16	78.66 \pm 1.57
FPH-GIN	78.80 \pm 3.89	44.67 \pm 5.57	79.08 \pm 2.45

6.5 Runtime and scalability

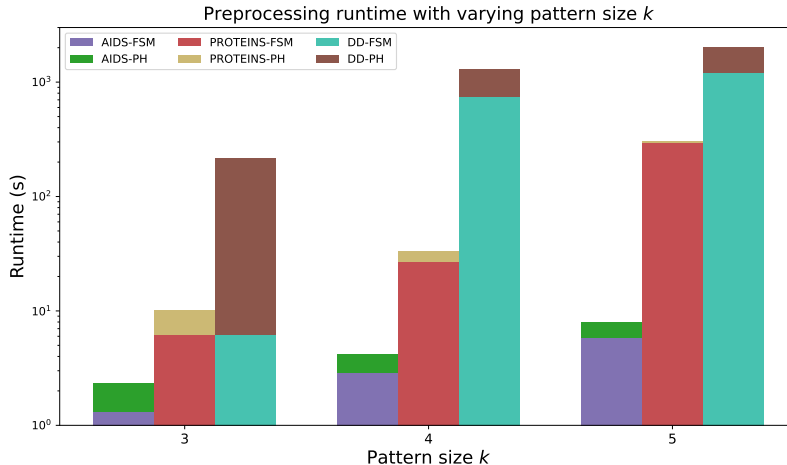
In this section, we evaluate the runtime and discuss the scalability of the proposed method. We first compare the component-wise and overall runtime of FPH-ML, FPH-GNN, DPH-ML, WL, and GCN across three datasets of different scales; among them, AIDS is the smallest, PROTEINS represents a medium scale, and DD is the largest. In this comparison, we set the maximum pattern size k of the FSM to 4, which allows the construction of nontrivial three-dimensional persistent homology. It is important to note that the pre-computation stage (FSM and PH calculation) of PH-based methods needs to be performed only a single time.

Table 8: Runtime comparison (in seconds) on three datasets. FSM and PH are executed once per training split as preprocessing.

Dataset	Method	FSM	PH	Train	Total
AIDS	FPH-ML	2.90	1.27	0.01	4.18
	FPH-GNN	2.90	1.27	36.41	40.58
	DPH-ML	–	0.39	0.02	0.41
	GCN	–	–	34.41	34.41
PROTEINS	FPH-ML	26.78	6.52	0.02	33.32
	FPH-GNN	26.78	6.52	39.41	72.71
	DPH-ML	–	2.04	0.03	2.07
	GCN	–	–	36.41	36.41
DD	FPH-ML	738.27	543.38	0.02	1281.67
	FPH-GNN	738.27	543.38	181.41	1463.06
	DPH-ML	–	6.05	0.05	6.10
	GCN	–	–	178.41	178.41

As shown in Table 8, both FSM and FPH introduce noticeable computational overhead; however, the total cost remains manageable for all datasets evaluated. The persistent homology computation in FPH is substantially more expensive than that of DPH. The key reason is that FPH does not compute PH on the original graph structure but rather on a *subgraph-pattern-induced filtration* constructed from all frequent patterns identified during FSM. DPH relies solely on a degree-based filtration, which operates directly on the graph and produces only 0- and 1-dimensional topological features. Although significantly faster, DPH cannot capture higher-dimensional topological structures such as H_2 , which FPH is capable of representing due to its richer pattern-based filtration. This highlights a fundamental trade-off between computational efficiency and expressive topological power. The DD dataset exhibits much larger runtimes than AIDS and PROTEINS across all FPH-based methods. This is mainly due to its larger graph density, since the complexity of FSM grows quickly with the number of subgraphs and their embeddings. In addition, the resulting pattern-induced filtrations are much larger, leading to a more expensive PH computation.

Based on the runtime analysis above, the major computational overhead lies in the preprocessing stage. We further evaluate the sensitivity of the method with respect to the pattern size k used in FSM and the subsequent PH construction. To this end, we conduct experiments by varying k from 3 to 5. Figure 9 shows that the preprocessing cost increases as the pattern size k grows. Although larger patterns naturally incur higher computational overhead, the cost remains manageable for typical choices of k , and small datasets such as AIDS and PROTEINS remain efficient even at $k = 5$. Importantly, our earlier results indicate that most of the discriminative power already emerges at the 2-dimensional level (i.e., features from H_0 to H_2). Increasing k beyond this range significantly expands the mined pattern space and the induced simplicial complexes, but in many cases does not lead to any noticeable performance improvement. Therefore, meaningful topological information is captured at relatively small pattern sizes, which keeps the overall preprocessing cost under control.

Figure 9: Preprocessing runtime with varying k .

While the above results demonstrate the effectiveness and scalability of FSF, its practical use on large graph databases also requires controlling the cost of the preprocessing stage. We therefore consider a budget-controlled mining strategy in the following section.

6.6 Budget-controlled approximate FSM

Exact frequent subgraph mining provides a complete set of patterns, but its computational cost can become expensive in both runtime and memory, particularly on medium- and large-scale graph datasets. This issue is further exacerbated for node-labeled graphs with low label entropy, where a large number of subgraph embeddings may be generated during pattern growth.

Motivated by these scalability challenges, we investigate a budget-controlled variant of frequent subgraph mining that explicitly limits the number of retained subgraph embeddings for each pattern-growth process. We evaluate this strategy on two datasets with distinct characteristics: PROTEINS, a medium-scale dataset with low node-label entropy, and ogbg-molhiv, a large-scale graph dataset with a substantially larger number of graphs. Figure 10 reports the preprocessing runtime, peak resident set size (RSS), and the number of discovered frequent subgraphs under different embedding budgets, normalized by the exact mining result with pattern size $k = 5$. The absolute cost of exact mining is summarized in Table 9.

Table 9: Cost of exact preprocessing.

Dataset	FSM Runtime (s)	PH Runtime (s)	Total Runtime (s)	Peak RSS (GB)	#Frequent
PROTEINS	298.0	14.2	312.2	1.31	883
ogbg-molhiv	617.6	31.1	648.7	1.87	674

According to the results shown in Figure 10, as the embedding budget increases, the preprocessing runtime, peak memory consumption, and the number of discovered frequent subgraphs all grow steadily, approaching the cost of exact mining. This trend is consistent across both datasets, indicating that the budget parameter effectively controls the computational complexity of the mining process. These results demonstrate that budget-controlled FSM provides a flexible mechanism to balance computational efficiency and information coverage.

To further assess the impact of embedding budget on downstream performance, we evaluate FPH-ML on the PROTEINS dataset under different budget settings. Since FPH-ML relies solely on FPH features without additional representation learning, it provides a direct and sensitive perspective for examining the effect of budget control. Table 10 reports the corresponding classification results. Notably, restricting the number of retained subgraph embeddings does not necessarily degrade downstream performance. In particular, budgets of 5k and 20k (highlighted in bold) achieve accuracy comparable to that of exact mining, indicating that a relatively small subset of subgraphs is sufficient to capture the discriminative topological information required for classification. Moreover, the non-monotonic perfor-

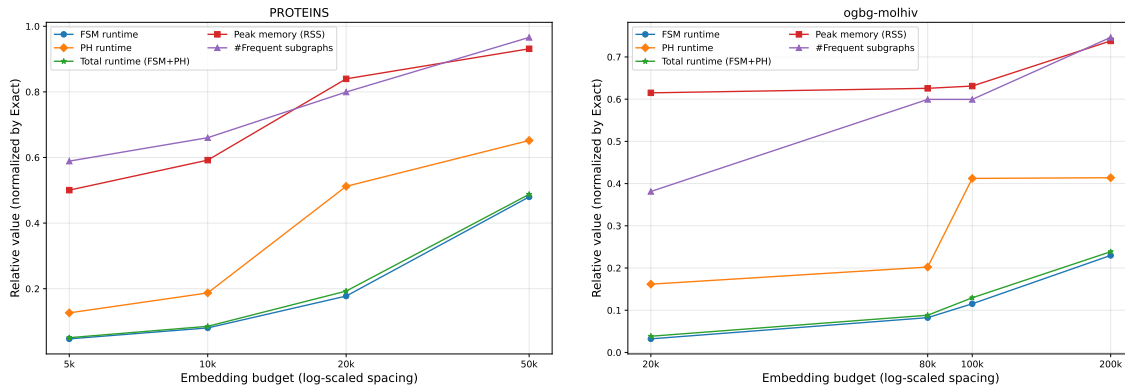


Figure 10: Effect of embedding budget on frequent subgraph mining and FPH calculation for PROTEINS (left) and ogbg-molhiv (right).

mance trend suggests that including additional subgraphs may introduce redundant or weakly discriminative patterns, highlighting the regularization effect of budget-controlled mining.

Table 10: Graph classification accuracy (%) of FPH-ML on the PROTEINS dataset under different embedding budgets. Results are reported as mean \pm standard deviation over 10 folds.

Embedding Budget	Accuracy (%)
Exact	74.31 \pm 4.78
50k	72.96 \pm 3.32
20k	73.86 \pm 2.92
10k	71.08 \pm 3.49
5k	73.86 \pm 2.39

7 Limitations and future directions

Despite these strengths, the proposed method still has several limitations. In particular, it inherits computational challenges from both frequent subgraph mining (FSM) and persistent homology (PH), and it is not directly applicable to dynamic or evolving graph datasets. We highlight several promising directions to address these challenges.

First, beyond efficiency-oriented approximations, future work may explore *topology-preserving approximate FSM* methods that prioritize subgraphs not only by frequency, but also by their contribution to preserving persistent homological features of the original graphs. Second, applying *graph coarsening* prior to FSM, while guaranteeing topological similarity to the original graph, may reduce both the search space and the size of the induced filtration. Third, incorporating *incremental or dynamic FSM* would enable efficient updates when new graphs arrive, making the framework suitable for streaming or evolving datasets without requiring re-mining from scratch. Finally, future work may explore *end-to-end differentiable variants* of FPH by integrating learnable filtrations or neural estimators of pattern importance, enabling joint optimization with downstream tasks and potentially improving both efficiency and performance.

From a theoretical perspective, we plan to further study the stability properties of frequent subgraph-based filtrations. In addition, we aim to better understand the topological interplay between frequent patterns and their induced PH features.

8 Conclusions

We propose a novel filtration, FSF, for computing persistent homology on graphs. It is the first filtration constructed from frequent subgraph patterns mined across the entire dataset, and we also provide the theoretical analysis of its properties. In particular, we show that persistence obtained from FSF reflects both the frequency of patterns and the topology of the graph. FSF enriches the set of PH filtrations and bridges FSM with TDA for graph classification.

Beyond persistent homology itself, we propose two approaches, FPH-ML and FPH-GNN, to incorporate the proposed PH features into graph classification. Extensive experiments on multiple benchmark datasets show that our methods outperform kernel-based, GNN-based, and PH-based baselines in most cases, highlighting the benefit of injecting high-order topological features into graph classification models.

References

- [1] Adams, H., Emerson, T., Kirby, M., Neville, R., Peterson, C., Shipman, P., Chepushtanova, S., Hanson, E., Motta, F., Ziegelmeier, L., 2017. Persistence images: A stable vector representation of persistent homology. *J. Machine Learning Research* 18, 1–35.
- [2] Aktas, M.E., Akbas, E., Fatmaoui, A.E., 2019. Persistence homology of networks: methods and applications. *Appl. Netw. Sci.* 4, 61:1–61:28.
- [3] Aslay, Ç., Nasir, M.A.U., Morales, G.D.F., Gionis, A., 2018. Mining frequent patterns in evolving graphs, in: *Proc. of the 27th ACM Intern. Conf. on Information and Knowledge Management, CIKM*, pp. 923–932.
- [4] Chen, X., Cai, J., Chen, G., Gan, W., Broustet, A., 2024. FCSG-Miner: Frequent closed subgraph mining in multi-graphs. *Information Sciences* 665, 120363.
- [5] Chen, Z., Chen, X., Chen, G., Gan, W., 2023. Frequent subgraph mining in dynamic databases, in: *IEEE Intern. Conf. on Big Data, BigData*, pp. 5733–5742.
- [6] Chowdhury, S., Mémoli, F., 2018. A functorial dower theorem and persistent homology of asymmetric networks. *J. Applied and Computational Topology* 2, 115–175.
- [7] Corcoran, P., Jones, C.B., 2023a. Topological data analysis for geographical information science using persistent homology. *International J. Geographical Information Science* 37, 712–745.
- [8] Corcoran, P., Jones, C.B., 2023b. Topological data analysis for geographical information science using persistent homology. *Int. J. Geogr. Inf. Sci.* 37, 712–745.
- [9] Edelsbrunner, H., Harer, J., et al., 2008. Persistent homology—a survey. *Contemporary mathematics* 453, 257–282.
- [10] Elseidy, M., Abdelhamid, E., Skiadopoulos, S., Kalnis, P., 2014. GRAMI: frequent subgraph and pattern mining in a single large graph. *Proc. VLDB Endowment* 7, 517–528.
- [11] Flammer, M., Hüper, K., 2024. Spatiotemporal persistence landscapes. *arXiv preprint 2412.11925*.
- [12] Fugacci, U., Scaramuccia, S., Iuricich, F., Floriani, L.D., 2016. Persistent homology: a step-by-step introduction for newcomers, in: *Proc. Conf. Smart Tools and Apps in Computer Graphics, STAG*, pp. 1–10.
- [13] Gilmer, J., Schoenholz, S.S., Riley, P.F., Vinyals, O., Dahl, G.E., 2017. Neural message passing for quantum chemistry, in: *Proc. Intern. Conf. on Machine Learning*, pp. 1263–1272.
- [14] Hamilton, W., Ying, Z., Leskovec, J., 2017. Inductive representation learning on large graphs. *Advances in neural information processing systems* 30.
- [15] He, C., Cai, J., Chen, G., Gan, W., 2025. A generic framework for mining sequences with various interestingness measures in dynamic attributed graphs. *Knowl. Inf. Syst.* 67, 6689–6716.
- [16] He, C., Chen, X., Chen, G., Gan, W., Fournier-Viger, P., 2024. Mining credible attribute rules in dynamic attributed graphs. *Expert Syst. with Appl.* 246, 123012:1–11.
- [17] Horn, M., De Brouwer, E., Moor, M., Moreau, Y., Rieck, B., Borgwardt, K., 2021. Topological graph neural networks. *arXiv preprint arXiv:2102.07835*.
- [18] Hu, W., Fey, M., Zitnik, M., Dong, Y., Ren, H., Liu, B., Catasta, M., Leskovec, J., 2020. Open graph benchmark: Datasets for machine learning on graphs. *Advances in neural information processing systems* 33, 22118–22133.
- [19] Immonen, J., Souza, A., Garg, V., 2023. Going beyond persistent homology using persistent homology. *Advances in neural information processing systems* 36, 63150–63173.
- [20] Inokuchi, A., Washio, T., Motoda, H., 2000. An apriori-based algorithm for mining frequent substructures from graph data, in: *Proc. European Conference on Principles of Data Mining and Knowledge Discovery*, pp. 13–23.
- [21] Ju, W., Mao, Z., Yi, S., Qin, Y., Gu, Y., Xiao, Z., Shen, J., Qiao, Z., Zhang, M., 2025. Cluster-guided contrastive class-imbalanced graph classification, in: *Proc. AAAI Conference on Artificial Intelligence*, pp. 11924–11932.
- [22] Kashima, H., Tsuda, K., Inokuchi, A., 2004. Kernels for graphs, in: *Kernel methods in computational biology*, pp. 155–170.

- [23] Kipf, T.N., Welling, M., 2016. Semi-supervised classification with graph convolutional networks. arXiv preprint 1609.02907.
- [24] Kriege, N.M., Johansson, F.D., Morris, C., 2020. A survey on graph kernels. *Applied Network Science* 5, 6.
- [25] Liang, D., Xia, S., Zhang, X., Zhang, W., 2021. Analysis of brain functional connectivity neural circuits in children with autism based on persistent homology. *Frontiers in Human Neuroscience* 15, 745671.
- [26] Liu, X., Chen, J., Wen, Q., 2023. A survey on graph classification and link prediction based on GNN. arXiv preprint 2307.00865.
- [27] Morris, C., Kriege, N.M., Bause, F., Kersting, K., Mutzel, P., Neumann, M., 2020. TUDataset: A collection of benchmark datasets for learning with graphs. arXiv preprint 2007.08663.
- [28] Narayanan, A., Chandramohan, M., Venkatesan, R., Chen, L., Liu, Y., Jaiswal, S., 2017. graph2vec: Learning distributed representations of graphs. arXiv preprint 1707.05005.
- [29] Petri, G., Sciamiero, M., Donato, I., Vaccarino, F., 2013. Topological strata of weighted complex networks. *PloS one* 8, e66506.
- [30] Pham, P., Bui, Q.T., Nguyen, N.T., Kozma, R., Yu, P.S., Vo, B., 2025. Topological data analysis in graph neural networks: Surveys and perspectives. *IEEE Trans. Neural Networks and Learning Systems* 36, 9758–9776.
- [31] Preti, G., Morales, G.D.F., Bonchi, F., 2022. FreSCo: mining frequent patterns in simplicial complexes, in: *Proc. 22nd The Web Conference*, pp. 1444–1454.
- [32] Pun, C.S., Xia, K., Lee, S.X., 2018. Persistent-homology-based machine learning and its applications—a survey. arXiv preprint 1811.00252.
- [33] Ravishanker, N., Chen, R., 2021. An introduction to persistent homology for time series. *Wiley Interdisciplinary Reviews: Computational Statistics* 13, e1548.
- [34] Rehman, S.U., Khalil, M.I., Kundi, M., AlSaedi, T., 2024. A study on frequent subgraph mining approaches: Challenges and future directions. *Research Updates in Mathematics and Computer Science* 4, 33–63.
- [35] Shaul, Z., Naaz, S., 2021. cgSpan: Closed graph-based substructure pattern mining, in: *Proc. IEEE Intern. Conf. on Big Data*, pp. 4989–4998.
- [36] Shervashidze, N., Schweitzer, P., Van Leeuwen, E.J., Mehlhorn, K., Borgwardt, K.M., 2011. Weisfeiler-lehman graph kernels. *J. Machine Learning Research* 12.
- [37] Shervashidze, N., Vishwanathan, S., Petri, T., Mehlhorn, K., Borgwardt, K., 2009. Efficient graphlet kernels for large graph comparison, in: *Artificial intelligence and statistics*, pp. 488–495.
- [38] Shi, Z., Sun, S., Yang, G., Liu, Y., 2025. Two-view fusion graph neural networks for graph classification, in: *Proc. Intern. Conf. on Intelligent Computing*, pp. 185–196.
- [39] Veličković, P., Cucurull, G., Casanova, A., Romero, A., Lio, P., Bengio, Y., 2017. Graph attention networks. arXiv preprint 1710.10903.
- [40] Wadhwa, R.R., Dhawan, A., Williamson, D.F., Scott, J.G., 2018. A flat persistence diagram for improved visualization of persistent homology. arXiv preprint 1812.04567.
- [41] Xu, K., Hu, W., Leskovec, J., Jegelka, S., 2019. How powerful are graph neural networks?, in: *Proc. 7th Intern. Conf. on Learning Representations*, p. OpenReview.net.
- [42] Yan, X., Han, J., 2002. gSpan: Graph-based substructure pattern mining, in: *Proc. IEEE Intern. Conf. on Data Mining*, pp. 721–724.
- [43] Yan, Z., Zhao, Q., Ye, Z., Ma, T., Gao, L., Tang, Z., Wang, Y., Chen, C., 2025. Enhancing graph representation learning with localized topological features. *J. Machine Learning Research* 26, 1–36.
- [44] Ying, R., Fu, T., Wang, A., You, J., Wang, Y., Leskovec, J., 2024. Representation learning for frequent subgraph mining. arXiv preprint 2402.14367.
- [45] Zeghina, A.O., Leborgne, A., Ber, F.L., Vacavant, A., 2023. Multi-SPMiner: A deep learning framework for multi-graph frequent pattern mining with application to spatiotemporal graphs, in: *Proc. Intern. Conf. on Knowledge-Based and Intelligent Information & Engineering Systems (KES)*, pp. 1094–1103.
- [46] Zhao, Q., Ye, Z., Chen, C., Wang, Y., 2020. Persistence enhanced graph neural network, in: *Proc. Intern. Conf. on Artificial Intelligence and Statistics*, pp. 2896–2906.